Research paper

Seismic performance of an assembled monolithic concrete column

Shufeng Li[1], Hexiang Li[2], Di Zhao[3]

Abstract: A prefabricated concrete column-to-column structure connected by high-strength bolts is proposed. To explore the seismic performance and failure form of the structure, the finite element analysis software is used to simulate the low-cycle repeated load test. The hysteretic curve and skeleton curve of the structure are obtained, and the stiffness degradation law, ductility and energy dissipation capacity of the structure are quantitatively analyzed to evaluate the seismic performance of the structure. The results show that the ductility coefficient of the structure is basically between 2.19 and 4.97, and the ductility coefficient of most specimens is greater than 3.0, indicating that the structure has good ductility and deformation capacity. The equivalent viscous damping coefficients of the specimens are in the range of 0.21–0.29, indicating that the structure has good energy dissipation capacity. In a certain range, increasing the thickness of the end plate has no significant impact on the energy consumption capacity of the structure. The compressive strength of the concrete in the core area is greatly improved under the constraint of the end plate bolts, and end plate bolt connection can well realize the transmission of force and give full play to the performance of materials.

Keywords: prefabricated concrete column, high strength bolt, end plate, ductility, energy dissipation capacity

[1]MSc, School of Civil Engineering, Xuchang University, Xuchang, 461000, China, e-mail: ll010720@126.com, ORCID: 0000-0001-8295-5879
[2]MSc, School of Civil Engineering, Xuchang University, Xuchang, 461000, China, e-mail: 350203409@qq.com, ORCID: 0009-0007-7798-6188
[3]MSc, School of Civil Engineering, Xuchang University, Xuchang, 461000, China, e-mail: 781862626@qq.com, ORCID: 0009-0008-7155-9297

1. Introduction

Concrete structures are dominant in the prefabricated buildings. The use of prefabricated concrete structures cannot only shorten the construction period and reduce construction difficulties, but also reduce the number of wet operations and workers on the construction site, thereby ensuring construction quality and saving costs. Through the investigation of earthquake damage, it was found that some large space assembly frame structures were severely damaged, mainly manifested as the connection failure between various prefabricated components, leading to structural dispersion or collapse during seismic events. These seismic damages indicate that the reliability of the node connection performance of existing prefabricated structures under repeated loads is poor, making it difficult to meet the actual requirements of earthquake resistance. Therefore, the application of prefabricated structures in seismic zones is greatly limited, making it important to study the seismic performance of prefabricated structural nodes. Many researches on prefabricated concrete joints have achieved optimal results [1–5]. Yamashita and Sanders [6] analyzed a full-scale prefabricated concrete column and a 1/4 scale prefabricated concrete column based on shaking table and finite element software. The aseismic performance of this prefabricated column was better. Seo et al. [7] experimentally studied the prefabricated concrete columns connected by steel sleeves. These studies mainly focused on the relationship between the bearing capacity and bonding force of steel bars and grouting materials in the sleeves. Rong and Luo [8] studied five prefabricated concrete columns connected by rolling straight thread sleeves and one cast-in-place concrete column. The aseismic performance of prefabricated concrete columns connected by rolling straight thread sleeves was equivalent to that of cast-in-place. Li et al. [9, 10] used high-strength spiral stirrups to confine concrete columns. The aseismic performance of this prefabricated column was basically the same as that of the cast-in-place column. Zhang et al. [11] proposed a new prefabricated column joint with clear force transmission and easy construction. This joint utilizes longitudinal bars and cogging structure of the column for connection. The seismic performance of the new column is largely equivalent to that of the cast-in-place column. This shows that, with proper design, the prefabricated column-to-column connection can achieve the same performance as the monolithic cast-in-place column. Taking the existing research into account, a fabricated concrete column-to-column structure that employs high-strength bolt connection is propose here. To explore the seismic performance of the structure, finite element software is established to analyze the seismic index of the structure. The overall structural content of this article mainly includes the establishment of a finite element model, comparative analysis of seismic performance (including hysteresis curve, skeleton curve, ductility coefficient, energy dissipation capacity, etc.), and stress analysis of each component.

2. Establishment of finite element model

2.1. Design of specimens

A total of 13 specimens (numbered as PYZ1-PYZ13) are designed. The main parameters are the axial compression ratio, concrete strength grade, bolt preload force, and end plate. The selection of axial compression ratio mainly considers the possibility of low, medium, and

high axial compression ratios in actual engineering. The selection of concrete grade is mainly based on commonly used low-strength concrete. The selection of bolt pre tightening force is based on the constraint effect of pre tightening force on concrete strength, and should not be too low or too high. If it is too low, the constraint effect may not be obvious; if it is too high, the concrete may be locally crushed. These parameters are the main factors affecting the bearing capacity of the section, which in turn have a significant impact on the seismic performance indicators of the structure, such as ductility and equivalent viscosity coefficient. The cross-sectional dimensions of the column are: the end-plate, the steel pipe and the concrete column are $700 \times 20 \times 480$ mm, 790×20 mm and $1450 \times 500 \times 500$ mm, respectively; the diameters of the bolt, steel bar and stirrup are 30 mm, 20mm and 5mm, respectively. The steel pipe and end plate are Q345 steel. High strength bolts with HRB400 reinforcement are selected. Basic parameters of the specimens are shown in Table 1.

Table 1. Basic parameters of specimens

No.	Concrete strength grade	Bolt preload force (kN)	Thickness of end plate (mm)	Axial compression ratio
PYZ-01	C40	200	20	0.3
PYZ-02	C40	150	20	0.3
PYZ-03	C40	300	20	0.3
PYZ-04	C40	400	20	0.3
PYZ-05	C30	200	20	0.3
PYZ-06	C35	200	20	0.3
PYZ-07	C50	200	20	0.3
PYZ-08	C40	200	15	0.3
PYZ-09	C40	200	25	0.3
PYZ-10	C40	200	30	0.3
PYZ-11	C40	200	20	0.4
PYZ-12	C40	200	20	0.5
PYZ-13	C40	200	20	0.7

2.2. Model establishment

When determining the boundary conditions, the lower end of the concrete column is fixed, that is, the lower end will restrict the translation and rotation in three directions. Coupling constraints are adopted at the top and bottom of the column to facilitate the application of load. The loading mode employed is displacement-controlled, with each stage being cycled once. C3D8R solid elements are used for concrete, end plates, steel pipes and bolts, and T3D2 truss

Table 2. Basic parameters of the concrete

Density (kg/m^3)	Poisson ratio μ	Expansion angle (Ψ)	Offset value (ε)	Strength value (α_f)	Ratio (K)	Viscosity coefficient (ν)
2.50×10^3	0.2	30	0.1	1.16	0.66667	5.0×10^3

Table 3. Basic parameters of the steel

Specimens	Density (kg/m^3)	Elastic Modulus (MPa)	Poisson ratio μ	Yield strength (MPa)	Ultimate strength (MPa)
Steel pipe	7.80×10^3	2×10^5	0.3	345	450
End-plate	7.80×10^3	2×10^5	0.3	345	450
Steel bar	7.80×10^3	2×10^5	0.3	400	450
Stirrup	7.80×10^3	2×10^5	0.3	1250	1100
High strength bolt/nut	7.80×10^3	2×10^5	0.3	1080	1150
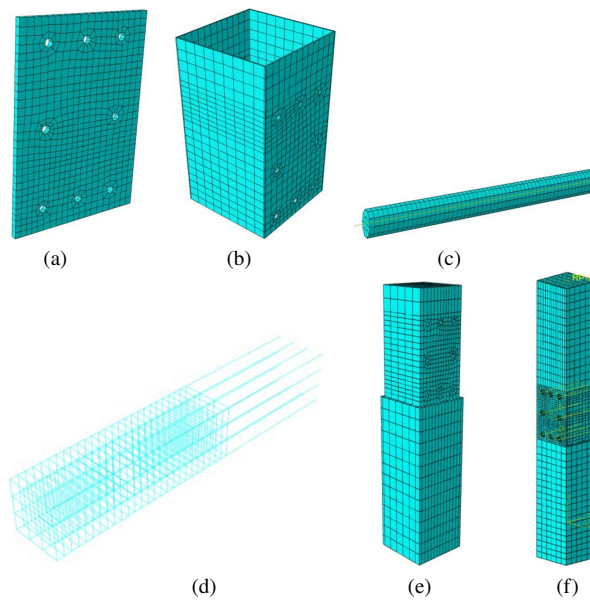
Fig. 1. Model grid division diagram; (a) End plate, (b) Steel pipe, (c) Bolt, (d) Upper reinforcement cage, (e) Concrete column, (f) Overall structure model

elements are used for reinforcement and stirrups. The interaction between the reinforcement and the concrete is defined as "embedded".

The tangential direction between the end plate and the steel pipe, as well as the steel hoop and the column is defined as friction contact. A penalty function is used to model this contact. The tangential contact between the bolt and the stud, as well as the ferrule and the end plate is defined as frictional contact, and the friction coefficient of the penalty function is 0.6 [12, 13]. The reinforcement adopts the double broken line model, while the concrete adopts the plastic damage model [14, 15]. The basic parameters of concrete and steel are shown in Table 2 and Table 3, respectively. The selection of grids mainly depends on the stress characteristics of the structure, and the grid division of key parts of the structure is denser [16, 17]. The boltgrid, the steel pipe and the end plate are 10 mm, 35 mm and 50 mm, respectively. The grid of the concrete column is 50 mm, and its division is shown in Fig. 1.

3. Comparative analysis of seismic performance

3.1. Load displacement hysteresis curve

The load-displacement hysteresis curve of each specimen is shown in Fig. 2.
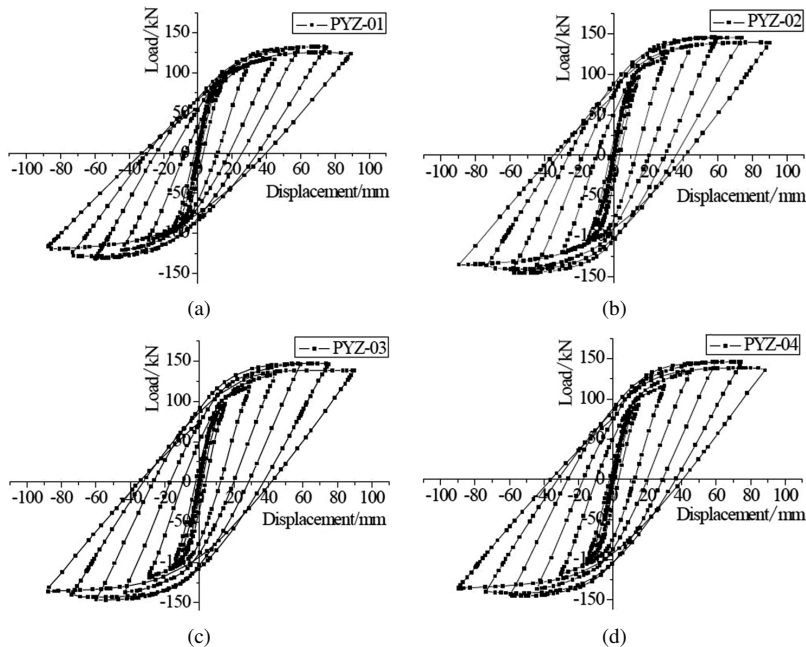

Fig. 2. Load-displacement curve of each specimen; (a) PYZ-01, (b) PYZ-02, (c) PYZ-03, (d) PYZ-04, (e) PYZ-05, (f) PYZ-06, (g) PYZ-07, (h) PYZ-08, (i) PYZ-09, (j) PYZ-10, (k) PYZ-11, (l) PYZ-12, (m) PYZ-13
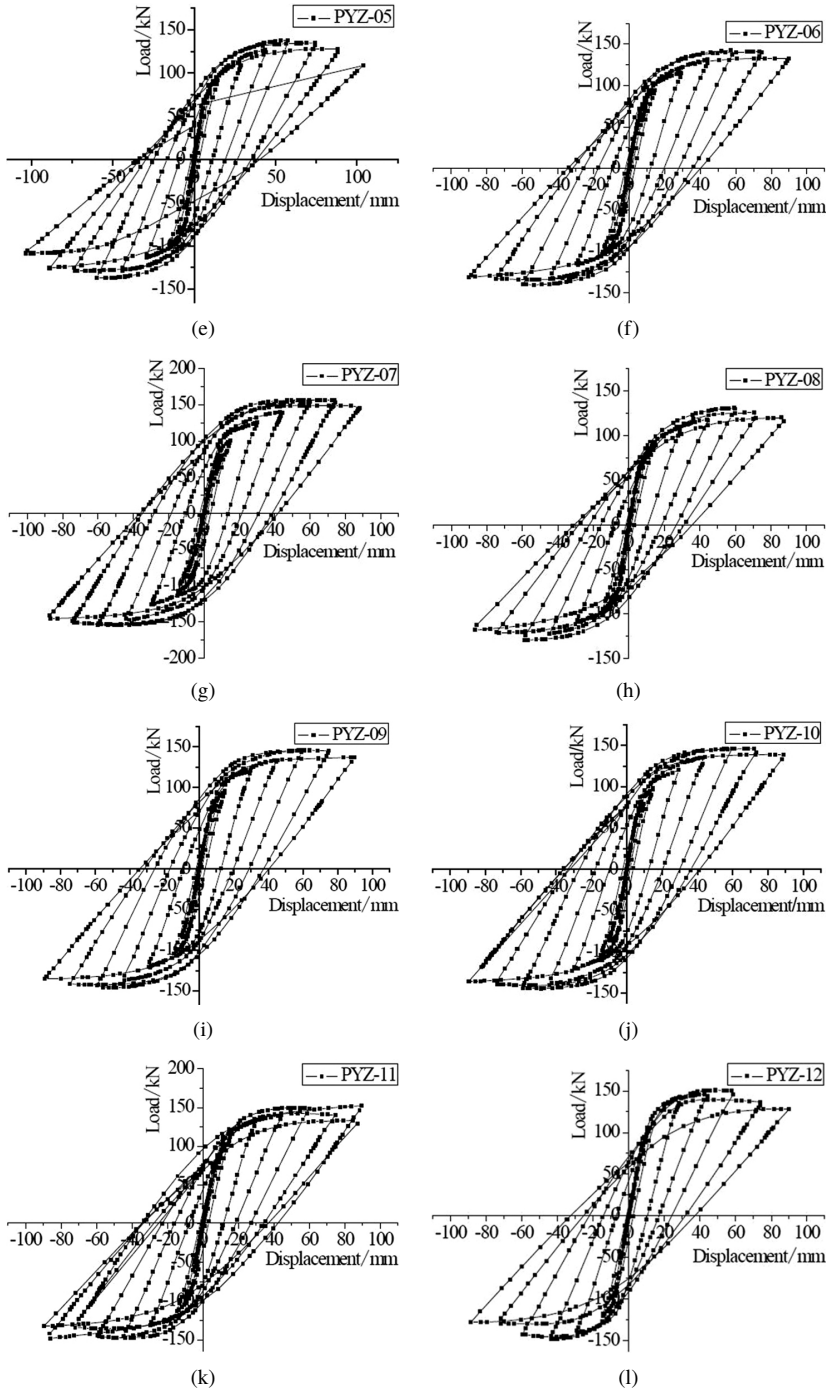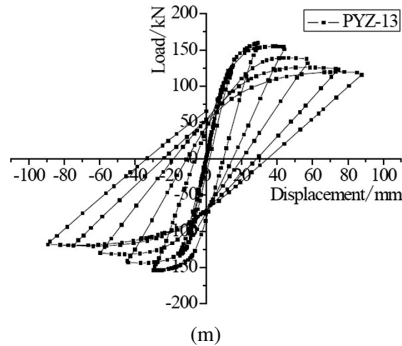
Fig. 2. [cont.]

(m)

Fig. 2. [cont.]

As shown in Fig. 2, during loading, the hysteresis curves of the 13 models are similar, basically between shuttle and bow. The main performance is: the loading in the initial stage is small; the load-displacement curve is similar to a straight line and the curve is almost coincident along the similar path of loading during unloading. As the displacement increases, the load increases slowly, and the stiffness decreases to a certain extent. In the later stage of loading, the load on the top of the column reaches its peak and the hysteresis curve "pinches". The area of hysteresis loop decreases, but is still in a shuttle shape, indicating that the energy dissipation capacity in the failure stage is good.PYZ-01, PYZ-05, PYZ-06 and PYZ-07 are similar but with different performance. Compared with PYZ-01, PYZ-05 and PYZ-06, the peak load of high-strength concrete specimen PYZ-07 increases by 18.08%, 13.20% and 9.69% respectively, indicating that the strength of high-strength concrete can improve the bearing capacity. Compared with PYZ-01, PYZ-08 and PYZ-09, the peak load of the high axial compression ratio specimen PYZ-10 increases by 10.86%, 11.82% and 0.06%, respectively, indicating that the thicker the end plate, the stronger the structural bearing capacity. The peak load of PYZ-13 with a high axial compression ratio is 2.61%, 3.35% and 17.18% higher than that of PYZ12, PYZ-11 and PYZ01, respectively, indicating that the high axial compression ratio has a large beneficial effect on the bearing capacity of the structure.

3.2. Skeleton curve

The skeleton curve comparison diagram of the specimens under different parameters is shown in Fig. 3.

Figure 3 shows that the growth of the skeleton curves at different bolt preloads is basically the same. Before yielding, the skeleton curve is close to a straight line. Subsequently, the four structures all yield at 18 mm, and the slope of the skeleton curves gradually decreases. As the load increases, the displacement increases, and the maximum bearing capacity is obtained at 60 mm. After exceeding the maximum load, the bearing capacity of the specimens gradually decreases with the failure and deformation of the concrete at the column end and core area. The growth of the skeleton curves with different concrete strengths is basically the same, and
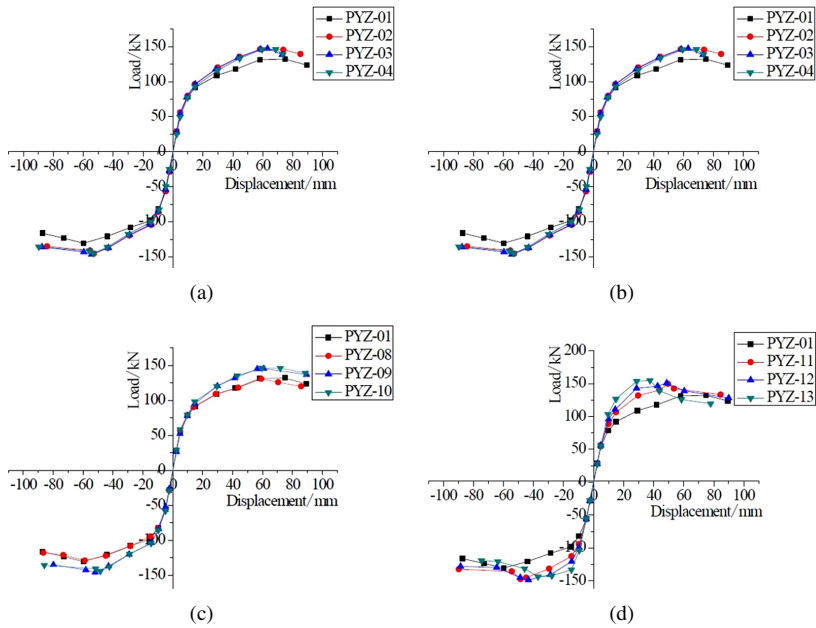
Fig. 3. Comparison diagram of skeleton curve under different parameters; (a) Under different bolt preloads, (b) Under different concrete strength, c) Under different end plate thickness, (d) Under different axial compression ratios

the maximum bearing capacity is obtained at 60 mm (PYZ-01/PYZ-05/PYZ-06) and 75 mm (PYZ-07). After that, with the failure and deformation of the concrete, the bearing capacity gradually decreases. The peak load of PYZ-07 is 13.21% higher than that of PYZ-05. Generally, the higher the strength grade of concrete, the higher of its bearing capacity. The greater the thickness of the end plate, the slower the bearing capacity decreases after yielding. The end plate restrains the deformation of the structure and can effectively restrain the deformation of the concrete. When the thickness of the end plate is 15 mm and 20 mm, 25 mm and 30 mm, the skeleton curves of the two are basically the same. However, compared with the thickness of 15 mm and 20 mm of the end plate, its bearing capacity is greatly improved, and the peak load increases by about 11.82%. This indicates that, increasing the thickness of the end plate within a certain range can effectively improve the bearing capacity of the structure. Under different axial compression ratios, the maximum bearing capacity of each specimen is obtained at 35 mm (PYZ-13), 45 mm (PYZ-11/PYZ-12) and 75 mm (PYZ-13), respectively, and the peak value of PYZ-13 is 17.18% higher than that of PYZ-01.

3.3. Ductility coefficient

Ductility is an important index in the seismic performance of structures, reflecting the plastic deformation capacity of structures or components [18]. Here the displacement ductility coefficient μ is for measurement.

(3.1)
$$\mu = \frac{\Delta_u}{\Delta_y}$$

where Δ_u is the failure displacement, referring to the displacement corresponding to the failure load; Δ_y is the yield displacement of specimens, determined by "PARK" method.

The characteristic point loads of each model and the corresponding horizontal displacement and displacement ductility coefficient of the column top are shown in Table 4.

Table 4. Displacement and ductility coefficient corresponding to the load of each characteristic point of each specimen

No.		Yield load P_y (kN)	Yield displacement Δ_y (mm)	Ultimate load P_u (kN)	Failure displacement Δ_u (mm)	Ductility coefficient μ
PYZ-01	Positive	105.51	26.66	132.74	89.42	3.35
	Negative	−102.76	−20.00	−129.89	−87.29	4.36
PYZ-02	Positive	117.79	28.71	146.69	85.18	2.97
	Negative	−112.39	−24.11	−144.83	−84.18	3.49
PYZ-03	Positive	119.67	30.24	147.58	73.04	2.42
	Negative	−113.28	−24.46	−144.83	−87.56	3.58
PYZ-04	Positive	121.34	33.59	146.69	73.51	2.19
	Negative	−114.16	−25.92	−143.94	−89.66	3.46
PYZ-05	Positive	108.16	27.89	137.95	88.19	3.16
	Negative	−108.07	−23.26	−136.08	−88.85	3.82
PYZ-06	Positive	114.36	28.32	143.15	89.94	3.18
	Negative	−108.95	−22.43	−138.73	−89.88	4.01
PYZ-07	Positive	125.64	30.75	156.64	88.22	2.87
	Negative	−120.47	−24.09	−154.51	−86.86	3.61
PYZ-08	Positive	103.92	24.82	130.75	85.84	3.46
	Negative	−101.64	−21.26	−127.65	−86.55	4.07
PYZ-09	Positive	116.91	27.73	145.81	89.48	3.23
	Negative	−114.16	−23.83	−145.71	−79.86	3.35
PYZ-10	Positive	119.57	30.05	147.58	88.70	2.95
	Negative	−109.84	−19. 18	−143.94	−85.90	4.48
PYZ-11	Positive	122.22	24.75	150.23	84.57	3.42
	Negative	−117.70	−18.60	−145.60	−89.77	4.83
PYZ-12	Positive	126.54	21.33	151.12	89.96	4.22
	Negative	−122.91	−18.32	−148.27	−88.56	4.83
PYZ-13	Positive	128.39	16.00	154.72	77.89	4.87
	Negative	−130.45	−15.02	−142.67	−74.61	4.97

From Table 4, the ductility coefficient of the assembled connecting column model is basically between 2.19 and 4.97, and the ductility coefficient of most specimens is greater than 3.0, indicating that each specimen has good ductility and deformation ability [19, 20] and meets the ductility requirements of RC structures. As the axial compression ratio increases, the ductility coefficients in positive and negative directions of the model increase. As such, improving the axial compression ratio of the structure can enhance the ductility and variability of structural joints.

3.4. Energy consumption index

The equivalent viscosity coefficients under different parameters are shown in Figure 4.
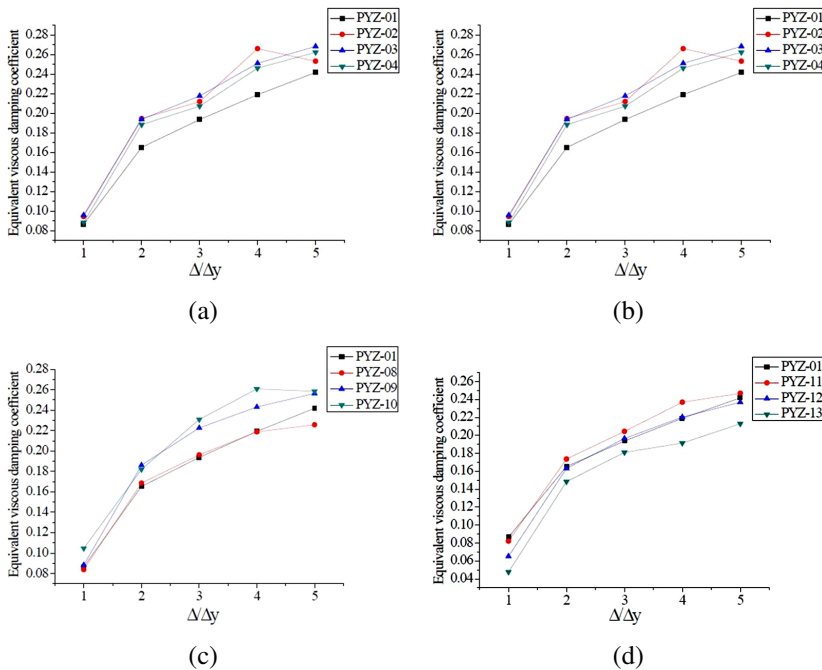
Fig. 4. Comparison of equivalent viscous damping coefficients of specimens under different parameters; (a) Under different bolt preloads, (b) Under different concrete strengths, (c) Under different end plate thicknesses, (d) Under different axial compression ratios

The equivalent viscous damping coefficient is 0.21–0.29. PYZ-07 has the strongest energy dissipation capacity, and the equivalent viscosity coefficient reaches 0.29, with optimal energy dissipation capacity [21, 22]. PYZ-02 and PYZ-10 decline downward in the last stage of loading, Figure 4 shows that as the bolt preload force increases, the energy dissipation capacity of the structure increases. The curves of the equivalent viscosity coefficient under different concrete strengths show that when the concrete strength grade is less than C50, the energy dissipation capacity of the structure does not increase significantly; when it is C50, the equivalent viscosity

coefficient increases significantly. This indicates the high-strength concrete has a significant beneficial effect on the energy dissipation capacity of the structure. The curves of equivalent viscosity coefficient under different end plate thicknesses show that when the thickness is 15 mm and 20 mm, basically the same [23]. When it is 25 mm and 30 mm, the equivalent viscosity coefficient increases significantly, indicating that increasing the thickness of the end plate has no significant effect on the energy dissipation capacity of the structure. When the thickness of the end plate exceeds a certain range, it will have a significant beneficial effect on the energy dissipation of the structure. From the equivalent viscosity coefficient curves of different axial pressure ratios, it can be seen that when the axial pressure ratio is less than 0.5, the equivalent viscosity coefficient curves are basically the same, with better energy dissipation capacity. When the axial pressure ratio is 0.7, the equivalent viscosity coefficient significantly declines, indicating that a high axial compression ratio has an adverse effect on the energy dissipation capacity of the structure.

4. Stress analysis of prefabricated concrete column-to-column connection structure

To explore the stress distribution of the structure at different stages, a specific analysis is conducted on the stress nephogram of PYZ-01 (Concrete grade C40; Bolt preload 200 kN; End plate thickness 20 mm; Axial compression ratio 0.3) in the yield state, limit state, failure state and loaded state.

4.1. Stress analysis of upper concrete column

Stress diagrams of the concrete columns at the upper end of the structure under different stages are shown in Figure 5.

It can be concluded from Fig. 5 that when the specimen yields, the strength of concrete in the core area reaches 50.6 MPa, higher than the strength grade of the concrete. This indicates that the strength of concrete in the core area is greatly improved under the constraint of the end

(a)   (b)
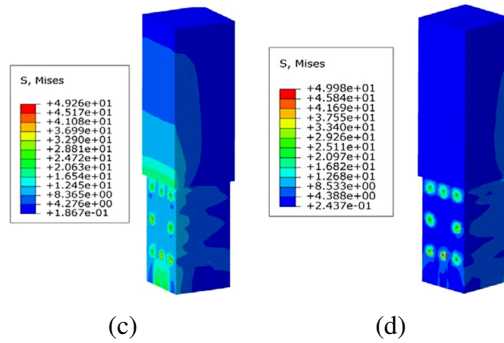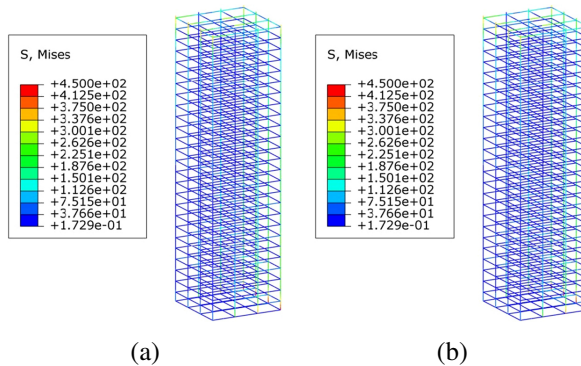
(c)   (d)
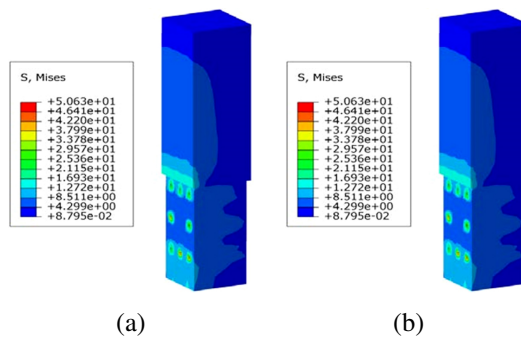
Fig. 5. Stress diagram of upper concrete at different stages; (a) Yield stage, (b) Ultimate stage, (c) Failure
stage, (d) Final stage

plates and high-strength bolts. At the same time, the maximum stress appears at the bolt hole, indicating that there will be a stress concentration at the bolt hole. When the specimen fails, the strength of concrete can still reach 49.3 MPa, indicating that the brittleness of concrete has been improved under 3D restraint. From the stress nephogram, it can be seen that the concrete in the core area bears a large force at both ends and a small force in the middle.

4.2. Stress analysis of reinforcement cage

The stress diagram of structural reinforcement cage at different stages is shown in Fig. 6.

As shown in Fig. 6, the lower end reinforcement cage experiences maximum stress concentrated near the core area of the structure. The maximum stress received by the stirrups in the failure stage reaches 1103 MPa (greater than the design yield strength by 1100 MPa and less than the design ultimate strength by 1250 MPa). However, the reinforcement experiences a stress of 645 MPa (greater than the design ultimate strength 450 MPa), indicating that it has undergone deformation due to yield failure.
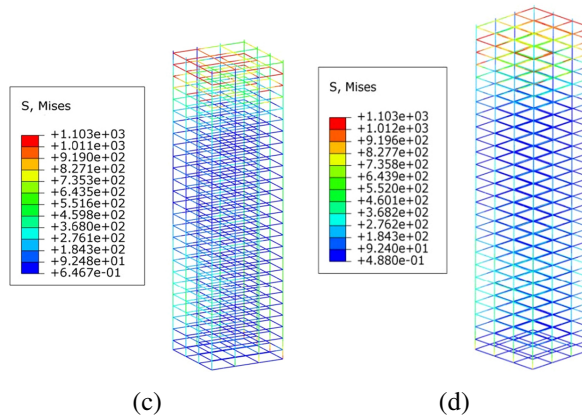

(a)   (b)

Fig. 6. Stress diagram of reinforcement cage at different stages; (a) Yield stage, (b) Ultimate stage, (c) Failure stage, (d) Final stage

5. Bolt stress analysis

The stress diagrams of structural bolts at different stages are shown in Fig. 7.
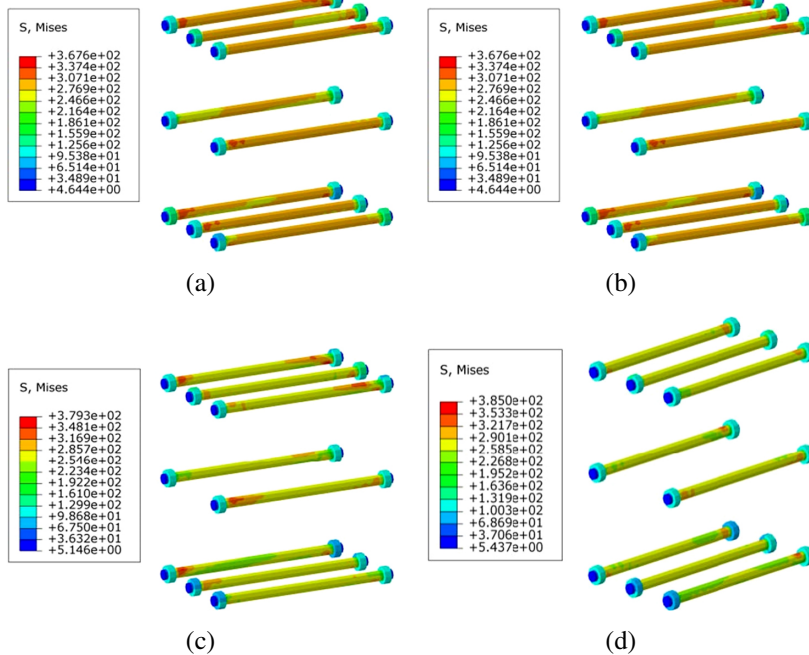

Fig. 7. Stress diagram of bolts at different stages; (a) Yield stage, (b) Ultimate stage, (c) Failure stage, (d) Final stage

Figure 7 shows that the maximum stress of bolt in the ultimate stage is 439 MPa, (far less than the designed yield strength 1080 MPa of the high-strength bolt). Therefore, the bolt did not reach the yield state, nor was it damaged, and its performance was optimal, playing a better role in transmitting loads.

5.1. End plate stress analysis

The stress diagrams of structural end plates at different stages are shown in Fig. 8.
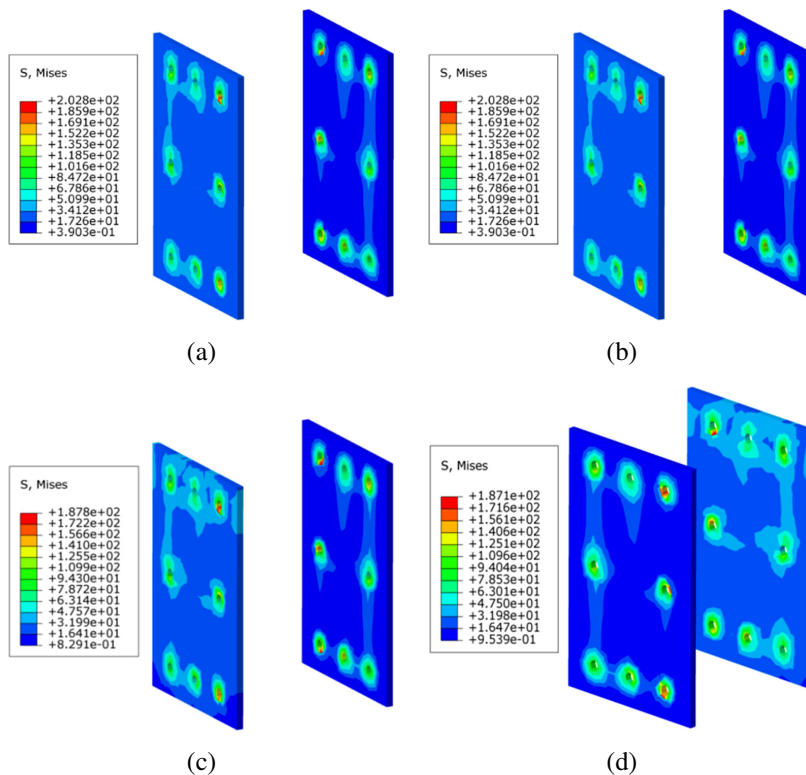

Fig. 8. Stress diagram of end plate at different stages; (a) Yield stage, (b) Ultimate stage, (c) Failure stage, (d) Final stage

Figure 8 shows that due to the bolt preload force, the stress in a small area near the bolt hole of the end plate is relatively concentrated, with strength of 203 MPa (less than the designed yield strength of the end plate 345 MPa). In other loading stages, the stress performance near the bolt hole is optimal, not exceeding 203 MPa, with good performance and better protection for the structure.

5.2. Stress analysis of steel pipe

The stress diagrams of structural steel pipes at different stages are shown in Fig. 9.

(a)   (b)

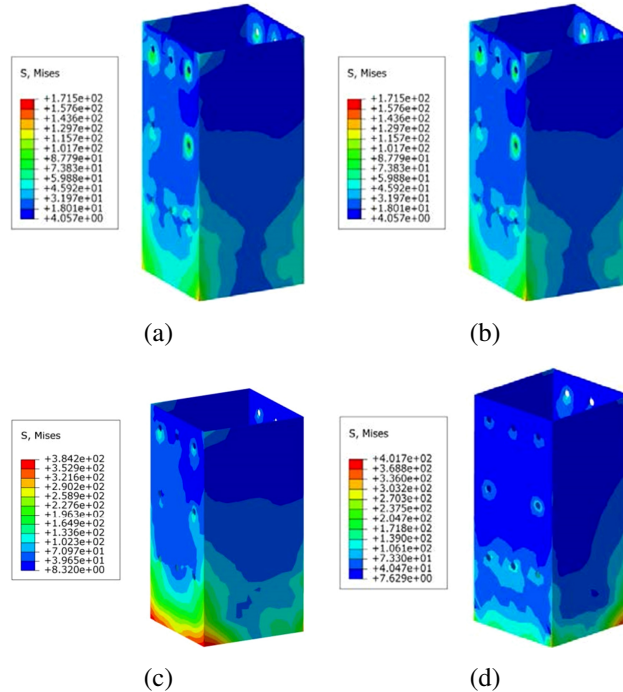(c)   (d)

Fig. 9. Stress diagram of steel pipe at different stages; (a) Yield stage, (b) Ultimate stage, (c) Failure stage, (d) Final stage

Figure 9 shows that the maximum stress of the steel pipe is concentrated near the core area of the joint. When the load is completed, the maximum stress of the steel pipe reaches 402 MPa (345 MPa higher than the designed yield strength of the steel pipe and 450 MPa less than the design ultimate strength of the steel pipe). Therefore, the steel pipe has reached a yield state without significant deformation, which can fully utilize the properties of the material and have good performance.

6. Conclusions

A fabricated concrete monolithic column structure connected by high-strength bolts is proposed. The pseudo static simulation experiments are conducted on 13 different models under different parameters using the finite element analysis software. The seismic performance of the fabricated monolithic column under different bolt preloads, concrete strength, end plate thickness and axial compression ratio is studied. The research results have obtained the

seismic performance indicators of the column, which can quantitatively evaluate its seismic performance and clearly show the main factors affecting seismic performance. In future practical engineering and seismic design, it can be used as a reference to determine whether to choose this type of structure and preliminarily screen the factors. The main conclusions and outlook are as follows:

1. The ductility coefficient of each specimen is basically between 2.19 and 4.97, and the ductility coefficient of most models is greater than 3.0. The equivalent viscous damping coefficient of each specimen at failure is 0.21–0.29 and has good energy dissipation capacity.

2. structure is improved. High strength concrete has an obvious beneficial effect on the energy dissipation capacity of the structure. When the thickness of the end plate exceeds a certain range, it will have a significant beneficial impact on the energy consumption of the structure. However, when the axial compression ratio is less than 0.5, the equivalent viscosity coefficient curves are basically the same. When the axial compression ratio is 0.7, the equivalent viscosity coefficient decreases significantly, indicating that the high axial compression ratio has an adverse impact on the energy dissipation capacity of the structure.

3. The stress nephogram of each component shows that the compressive strength of concrete in the core area is greatly improved under the constraint of the end plate bolts. End plate bolt connection can well realize the transmission of force and give full play to the performance of materials.

4. The current research on assembled integral concrete columns primarily examines their seismic performance. However, further investigation is required to develop design methods for section bearing capacity and components like end plates and bolts. Additional data can be gathered through experiments and finite element analysis to establish a restoring force model for the structure. This model will serve as a foundation for elastic-plastic analysis and overall structural design.

Acknowledgements

References

[1] R. Ketiyot and C. Hansapinyo, "Seismic performance of interior precast concrete beam-column connections with T-section steel inserts under cyclic loading", *Earthquake Engineering and Engineering Vibration*, vol. 17, no. 2, pp. 355–369, 2018, doi: 10.1007/s11803-018-0446-9.

[2] J.D. Nzabonimpa, W.K. Hong, and J. Kim, "Experimental and Nonlinear Numerical Investigation of the Novel Detachable Mechanical Joints with Laminated Plates for Composite Precast Beam-column Joint", *Composite Structures*, vol. 185, pp. 286–303, 2018, doi: 10.1016/j.compstruct.2017.11.024.

[3] S.C. Chen, F.Z. Zhu, W. Pang, and W.M. Yan, "Seismic behavior of post-tensioned precast RC beam-column joints with additional curved steel braces", *Journal of Building Structures*, vol. 41, no. 9, pp. 98–104, 2020, doi: 10.14006/j.jzjgxb.2018.0398.

[4] J.L. Zhang, J. Li, X.C. Zheng, H.J. Zhao, and Q.N. Li, "Analysis of collapse resistance of prefabricated RC frame structure with reinforcement connection", *Journal of Harbin Institute of Technology*, vol. 53, no. 4, pp. 111–119, 2021, doi: 10.11918/202005078.

[5] X.J. Wang and Q. An, "Research on flexural bearing capacity of fabricated beam-column outer ring-plate high-strength bolted joints", *Industrial Construction*, vol. 50, no. 11, pp. 125–132, 2020, doi: 10.13204/j.gyjzG20070605.

[6] R. Yamashita and D.H. Sanders, "Seismic Performance of Precast Unbonded Prestressed Concrete Columns", *ACI Structural Journal*, vol. 106, no. 6, pp. 821–830, 2009, doi: 10.14359/51663183.

[7] S.Y. Seo, B.R. Nam, and S.K. Kim, "Tensile Strength of the Grout-filled Head-splice-sleeve", *Construction and Building Materials*, vol. 124, pp. 155–166, 2016, doi: 10.1016/j.conbuildmat.2016.07.028.

[8] Q. Rong and Q. Luo, "Experimental Study on Seismic Performance of an Improved Precast Reinforced Concrete Column-to-Column Joint", *Mechanics Based Design of Structures and Machines*, vol. 50, no. 5, pp. 1760–1777, 2022, doi: 10.1080/15397734.2020.1763183.

[9] J. Li, Z. Liu, Q.N. Li, and X.J. Li, "Test research on seismic performance of new-type assembled monolithic short columns", *World Earthquake Engineering*, vol. 30, no. 1, pp. 29–33, 2014.

[10] J. Li, P. Chen, W. Wei, and Q. N. Li, "Seismic behavior research of steel plate hoop-bolt prefabricated column confined by high-strength composite spiral stirrups", *Industrial Construction*, vol. 44, no. 7, pp. 7–10, 2014, doi: 10.13204/j.gyjz201407002.

[11] J.Y. Zhang, H. Wang, J.Z. Wang, and Y. Zhu, "Theoretical analysis and numerical simulation of a novel precast concrete column-column joint", *Industrial Construction*, vol. 49, no. 1, pp. 85–90+114, 2019, doi: 10.13204/j.gyjz201901015.

[12] Q. Wang, J. Lu, K.K. Hou, and Z.P. Yin, "Study of Material Constitutive Model for Shear Wall Hysteretic Behavior Analysis", *Journal of Shenyang Jianzhu University (Natural Science)*, vol. 34, no. 3, pp. 402–409, 2018.

[13] W.Y. Zhang and Y.Y. Chen, "Effect of the Hardening Parameters in Steel Constitutive Models on the Hysteretic Behavior of Structural Members", *Progress in Steel Building Structures*, vol. 19, no. 1, pp. 10–16, 2017, doi: 10.13969/j.cnki.cn31-1893.2017.01.002.

[14] GB50010-2010 Code for Design of Concrete Structures. China Architecture and Building Press, Beijing, China, 2010.

[15] Y. Qing, Y. Yuan, C.L. Wang, S.P. Meng, and B. Zeng, "Experimental study of precast columns with a hybrid joint incorporating bolted couplers and grouted sleeves", *Journal of Building Engineering*, vol. 49, art. no. 106878, 2023, doi: 10.1016/j.jobe.2023.106878.

[16] S. Kalmykova, "Simulation of t-joints between rhs steel members with offset in ABAQUS CAE", *Acta Polytechnica CTU Proceedings*, vol. 30, pp. 36–40, 2021, doi: 10.14311/APP.2021.30.0036.

[17] H.B. Chen, Y.J. Zhou, and N. Ge, "Seismic Performance Research for L-shaped Column Joint with Concrete Filled Steel Pipe Based on ABAQUS Software", *Earthquake Resistant Engineering and Retrofitting*, vol. 39, no. 2, pp. 24–29, 2017, doi: 10.16226/j.issn.1002-8412.2017.02.004.

[18] JGJ101-2015 Specification of Testing Methods for Earthquake Resistant Building. China Architecture and Building Press, Beijing, China, 2015.

[19] D. Zenunović and R. Folić, "Models for behavior analysis of monolithic wall and precast or monolithic floor slab connections", *Engineering Structures*, vol. 40, pp. 466–478, 2012, doi: 10.1016/j.engstruct.2012.03.007.

[20] Y.H. Cao, H. Jin, and H. Jiang, "Research on new beam column joints of fully prefabricated concrete frame structure", *Construction Technology*, vol. 49, no. 5, pp. 29–33+84, 2020.

[21] L. Wang, S.J. Yan, Y. Zheng, and C.L. Zhang, "Tests on seismic behavior of joints in steel frame with steel-concrete composite beams", *Journal of Harbin Institute of Technology*, vol. 46, no. 4, pp. 1–6, 2014.

[22] N. El-Joukhadar, F. Dameh, and S. Pantazopoulou, "Seismic Modelling of Corroded Reinforced Concrete Columns", *Engineering Structures*, vol. 275, art. no. 115251, 2023, doi: 10.1016/j.engstruct.2022.115251.

[23] B. Langier, J. Katzer, M. Major, J. Halbiniak, and I. Major, "Strength and durability characteristics of concretes with crushed side window glass as partial aggregate substitution", *Archives of Civil Engineering*, vol. 69, no. 2, pp. 5–21, 2023, doi: 10.24425/ace.2023.145249.